ACS APPLIED MATERIALS & INTERFACES

www.acsami.org

Research Article

Direct Imaging of Ion Migration in Amorphous Oxide Electronic Synapses with Intrinsic Analog Switching Characteristics

Atsushi Tsurumaki-Fukuchi,* Takayoshi Katase, Hiromichi Ohta, Masashi Arita, and Yasuo Takahashi

Cite This: *ACS Appl. Mater. Interfaces* 2023, 15, 16842−16852

Read Online

ACCESS | Metrics & More | Article Recommendations | Supporting Information

ABSTRACT: Amorphous metal oxides with analog resistive switching functions (i.e., continuous controllability of the electrical resistance) are gaining emerging interest due to their neuromorphic functionalities promising for energy efficient electronics. The mechanisms are currently attributed to field-driven migration of the constituent ions, but the applications are being hindered by the limited understanding of the physical mechanisms due to the difficulty in analyzing the causal ion migration, which occurs on a nanometer or even atomic scale. Here, the direct electrical transport measurement of analog resistive switching and ångström scale imaging of the causal ion migration is demonstrated in amorphous TaO_x (a-TaO_x) by conductive atomic force microscopy. Atomically flat thin films of a-TaO_x, which is a practical material for commercial resistive random access memory, are fabricated in this study, and the mechanisms of the three known types of analog resistive switching phenomena (current-dependent set, voltage-dependent reset, and time-dependent switching) are directly visualized on the surfaces. The observations indicate that highly analog type of resistive switching can be induced in a-TaO_x by inducing the continuous redox reactions for $2.0 < x < 2.5$, which are characteristic of a-TaO_x. The measurements also demonstrate drastic control of the switching stochasticity, which is attributable to controlled segregation of a metastable a-TaO_2 phase. The findings provide direct clues for tuning the analog resistive switching characteristics of amorphous metal oxides and developing new functions for future neuromorphic computing.

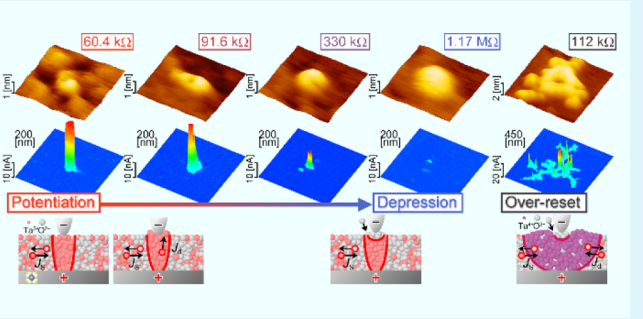

KEYWORDS: *analog resistive switching, electronic synapses, memristors, amorphous metal oxides, conductive atomic force microscopy, tantalum oxides*

1. INTRODUCTION

Continuous (nondiscrete) control of the resistance of a material has been vigorously pursued in recent neuromorphic (bioinspired) electronics as an important principle of electronic synapses, where biological synaptic weight changes are mimicked by resistance changes. Continuous resistance changes induced by electric field application, i.e., analog (or memristive) resistive switching phenomena, have been demonstrated in nanostructured amorphous metal oxides (TaO_x, HfO_x, etc.),[1−13] with advantages for applications (high neuromorphic functionality, low power consumption, and high scalability). The hardware development of oxide-based electronic synapses, however, has been hampered by the poorly understood physical mechanisms, which significantly limits function control. Recent research efforts have proposed phenomenological models of the mechanisms based on transport measurements and numerical simulations,[2,4,5,7−9,11−15] and the involvement of field-driven migration of constituent ions has been suggested by the models, while the details of the ion migration and origin of the switching continuity remain elusive.

Scanning probe microscopy observation of an analog resistive switching phenomenon has recently become an important challenge for understanding the intrinsic nature of switching because the atomic-scale ion migration that accounts for the switching continuity can potentially be observed. In fact, this methodology has been widely employed for investigating conventional (non-analog, discrete type) resistive switching phenomena,[16−24] and a few pioneering studies have also been reported for analog-type switching.[25−27] However, the mechanisms of the ion migration remain largely unproven because of the severe requirements on electrical input control and observation resolution for investigating a truly analog type of resistive switching. For examples, imaging of a conduction path and structural observations of the ion migration in a

Received: November 30, 2022
Accepted: March 13, 2023
Published: March 23, 2023

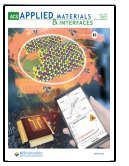

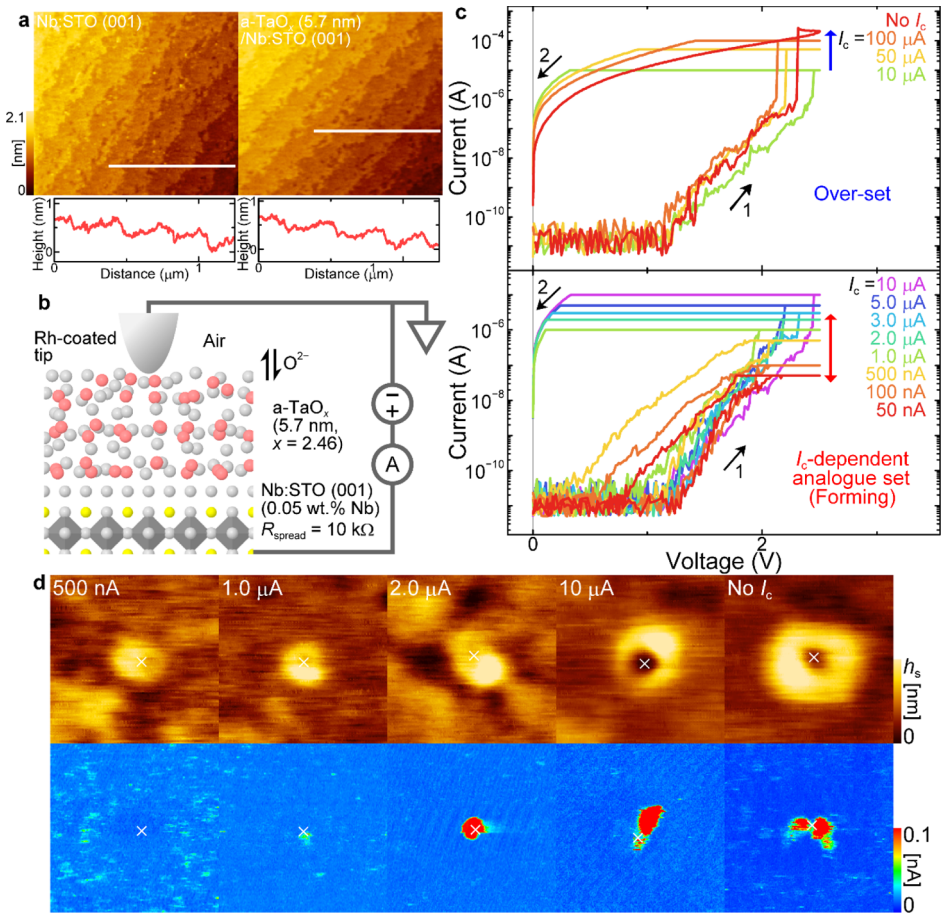

Figure 1. (a) Topographic AFM images of (left) a Nb:STO (001) substrate and (right) an a-TaO_x (5.7 nm) thin film deposited on it. The bottom figures show the surface profiles along the horizontal white lines in the images. (b) Schematic illustration of the experimental setup for C-AFM measurement of a-TaO_x thin films. (c) DC $I-V$ characteristics of an a-TaO_x thin film measured by C-AFM under I_c = 50 nA−100 μA and no I_c. The black arrows and numbers indicate the voltage sweeping sequence, and the red and blue arrows indicate the current ranges where the analog- and over-set switching was observed in the measurements, respectively. (d) (top) Topographic and (bottom) current C-AFM images of the a-TaO_x thin film observed directly after the C-AFM $I-V$ measurements with I_c = 500 nA−10 μA and without I_c. The scan area is 200 × 200 nm^2, and a reading voltage of −1.0 V was applied to acquire the current images. The height scales (h_ss) used for depicting the topographic images are 0.4, 0.5, 0.6, 0.9, and 0.8 nm for the images with I_c = 500 nA, I_c = 1.0 μA, I_c = 2.0 μA, I_c = 10 μA, and no I_c, respectively. The white crosses in the images mark the contact positions of the C-AFM tips in the $I-V$ measurements.

switching material have not yet been demonstrated for an analog type of switching phenomena by probe microscopy.

In this work, we directly visualized the mechanisms of the analog resistive switching phenomena in amorphous TaO_x (a-TaO_x) by optimized conductive atomic force microscopy (C-AFM) observation via fabricating its atomically flat thin films. We selected a-TaO_x as the target material in this study because it is currently considered a key material in resistive switching applications. A variety of neuromorphic functions, including high-performance analog resistive switching,[3−8,10,13] spike timing-dependent plasticity,[4,7] and second-order memristor characteristics,[7] have been demonstrated in thin-film devices of a-TaO_x, in addition to the fact that it has been widely used as a practical material for commercial resistive random access memory (ReRAM).[3,10,28] In amorphous metal oxides, three types of analog switching phenomena have been demonstrated depending on the control parameters: (1) analog set (resistance decrease) controlled by the compliance current (I_c),[1,5,6,13] (2) analog reset (resistance increase) controlled by the maximum applied voltage (V_{max}),[1,3,4,6,8,13] and (3) analog set and reset by multiple voltage applications (i.e., controlled by the voltage application time).[2,4,7,8] In our measurements, all three types of phenomena were directly demonstrated by C-AFM, and the involved ionic migration was observed in the ångström scale. The observations revealed that the analog resistive switching of a-TaO_x originates from complementary migration of the tantalum and oxide ions and suggested that its dominant cause distinctively varies with the control parameters and stages of switching, as exemplified by the electric drift, thermal diffusion, and continuous redox reactions (which are characteristics of a-TaO_x). Moreover, the measurements demonstrated that the stochasticity of the resistive switching can be drastically changed by simply turning the migration direction of the tantalum and oxide ions, and important involvement of the segregation of a metastable a-TaO_2 phase in the stochastic-type switching was suggested. These results provide direct insights into the physical origins of the analog and stochastic resistive switching in amorphous metal oxides and may enable us to directly design the properties toward neuromorphic and stochastic computing applications.

2. RESULTS AND DISCUSSION

2.1. Measurement Setup Using Atomically Flat a-TaO_x. For the C-AFM analyses, in this study, a-TaO_x thin films

https://doi.org/10.1021/acsami.2c21568
ACS Appl. Mater. Interfaces 2023, 15, 16842−16852

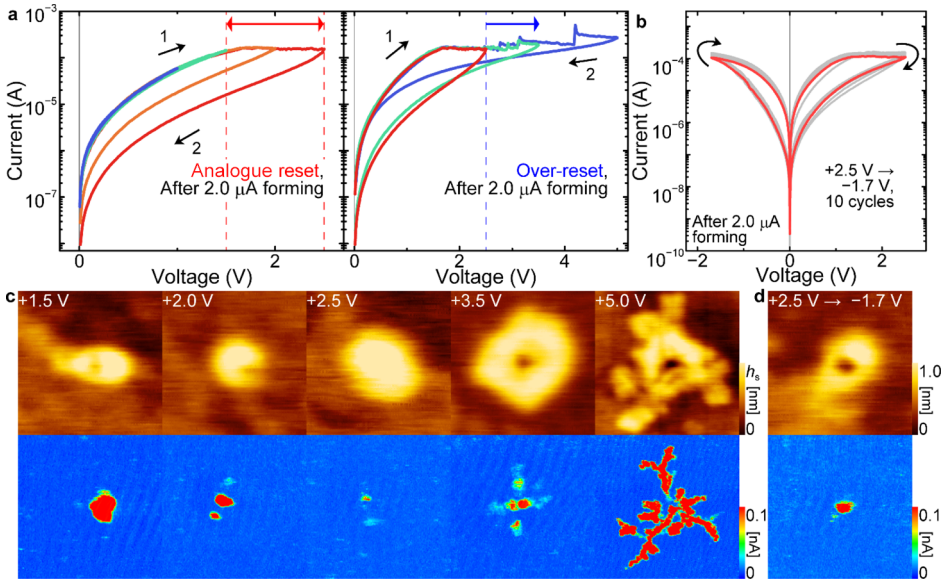

Figure 2. (a) DC $I-V$ characteristics of an a-TaO_x (5.7 nm) thin film measured after initial set operations at I_c = 2.0 μA by C-AFM with a V_{max} of (left) +1.0−+2.5 V and (right) +2.5−+5.0 V. The black arrows and numbers indicate the voltage sweeping sequence, and the red and blue arrows and dashed vertical lines indicate the voltage ranges where the analog- and over-reset switching was observed in the measurements, respectively. (b) DC $I-V$ characteristics of the a-TaO_x thin film measured by applying 10 voltage sweeping cycles of 0 → +2.5 → −1.7 → 0 V by C-AFM after an initial set operation at I_c = 2.0 μA. (c) (top) Topographic and (bottom) current C-AFM images observed directly after the C-AFM $I-V$ measurements of the first reset switching with a V_{max} of +1.5−+5.0 V. The scan areas are 200 × 200 nm^2 for the images with V_{max} = +1.5−+3.5 V and 450 × 450 nm^2 for the images with V_{max} = +5.0 V. A reading voltage of −1.0 V was applied to acquire the current images. The h_ss used for depicting the topographic images are 1.1, 1.3, 1.2, 1.4, and 1.6 nm for the images with V_{max} = +1.5, +2.0, +2.5, +3.5, and +5.0 V, respectively. (d) (top) Topographic and (bottom) current C-AFM images observed after set switching with V_{max} = −1.7 V (following the first reset switching with V_{max} = +2.5 V). The scan area is 200 × 200 nm^2, and a reading voltage of −1.0 V was applied to acquire the current image.

with atomically flat surfaces were fabricated by the pulsed laser deposition (PLD) method under oxygen partial pressures (P_{O2}s) of ≤6 Pa (see Supporting Information, Figure S1). When the a-TaO_x films were deposited on Nb-doped $SrTiO_3$ (Nb:STO) (001) substrates with atomically stepped surfaces, the periodical structures formed by the single-unit-cell-height (0.3905 nm) steps were nearly completely reproduced on the film surfaces (Figure 1a). The setup of our C-AFM measurements for the a-TaO_x (5.7 nm) thin films is shown in Figure 1b. The measurements were conducted in air, and voltages were applied from the biased Nb:STO (001) substrates to the grounded tips in all of the current−voltage ($I-V$), current−time ($I-t$), and current-mapping measurements by C-AFM. An external source measurement unit (B1500A, Keysight Co., Ltd.) was used in the $I-V$ and $I-t$ measurements to cover a wide range of currents involved in the resistive switching (from 10^{-11} to 10^{-3} A). The atomically flat surface of the a-TaO_x films and atmospheric C-AFM setup are considered particularly suitable for observing the analog-type switching phenomena (see the Experimental Section). The composition formula of the a-TaO_x films used for the C-AFM measurements was determined to be $TaO_{2.46}$ by X-ray photoelectron spectroscopy (Figure S2). The valence of the tantalum ions was thus suggested to be mostly +5 in the initial state.

In the following sections, we describe the detailed processes of the analog and stochastic resistive switching of a-TaO_x observed using this setup. The characteristics of the (1) current-dependent analog set and (2) voltage-dependent analog reset phenomenon are presented first, followed by a demonstration of stochasticity control of the resistive switching (based on control of the ion migration directions). The results on the (3) time-dependent analog switching phenomenon (investigated by multiple pulsed voltage applications) are then presented, and the suggested mechanism of each phenomenon is finally described.

2.2. C-AFM Observation of Current-Dependent Analog Set. DC $I-V$ characteristics measured on the pristine surface of an a-TaO_x (5.7 nm) thin film by C-AFM and topographic and current images observed directly after the C-AFM $I-V$ measurements are shown in Figure 1c,d. In the measurements, systematically regulated I_cs (horizontal straight parts in the plot of the characteristics) were applied to the a-TaO_x film using the measurement unit (B1500A semiconductor parameter analyzer). Clear initial set switching (so-called forming) and significant I_c dependence of the switched resistance, i.e., the (1) I_c-dependent analog set phenomenon,[5,6,13] were demonstrated in the $I-V$ characteristics. The measurements revealed that the current-dependent analog set of a-TaO_x is a multistep phenomenon, in which the I_c dependence of the switched resistance has critical currents of I_c = 1.0 and 10 μA. The switched resistance of the a-TaO_x film showed a sensitive dependence on the applied I_c for I_c <1.0 μA. In contrast, very small topographic deformation with a height of 0.3 nm and apparently no conductive area were observed in the C-AFM images after the measurements in this I_c range [Figures 1d and S3 for details (including the C-AFM images without white crosses for I_c = 500 nA−2.0 μA)]. Note that mutually different height scales (h_ss) are used for drawing the topographic images in Figure 1d to obtain better visualization results for the structures at lower I_cs (as well as in Figures 2c and 3c). For the topographic structures in the I_c-dependent analog set phenomenon, however, three-dimensional drawings with a constant topographic height scale are provided in Figure

https://doi.org/10.1021/acsami.2c21568
ACS Appl. Mater. Interfaces 2023, 15, 16842−16852

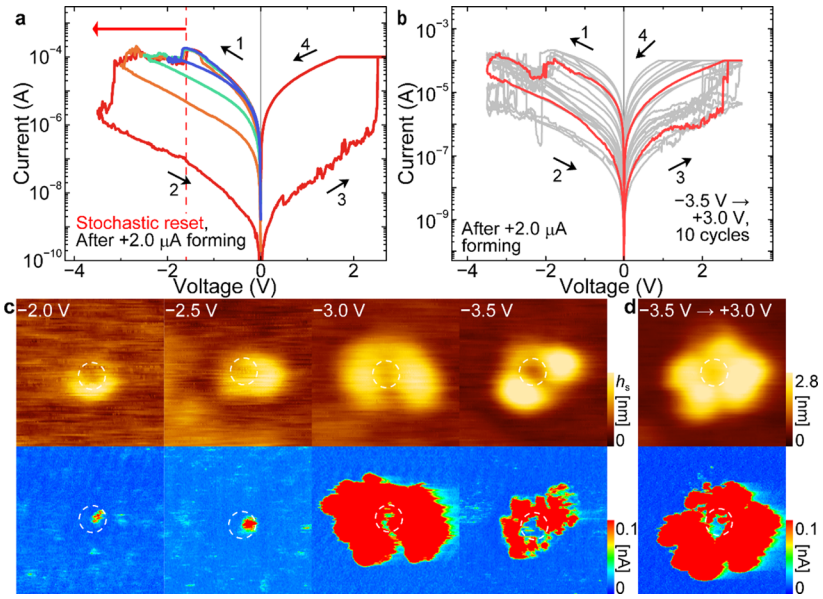

Figure 3. (a) DC $I-V$ characteristics of an a-TaO_x (5.7 nm) thin film measured with V_{max} = −2.0 to −3.5 V by C-AFM after initial set operations at I_c = 2.0 μA. The black arrows and numbers indicate the voltage sweeping sequence, and the red arrow and dashed vertical line indicate the voltage range where the stochastic-type reset switching was potentially observed in the measurements. A subsequent set operation with V_{max} = +3.0 V and I_c = 100 μA ("3" and "4") is also shown in the figure. (b) DC $I-V$ characteristics of the a-TaO_x thin film measured by applying 10 voltage sweeping cycles of 0 → −3.5 → +3.0 → 0 V under I_c = 100 μA for the set operations by C-AFM after an initial set operation at I_c = 2.0 μA. (c) (top) Topographic and (bottom) current C-AFM images observed directly after the C-AFM $I-V$ measurements of the first reset switching with V_{max} = −2.0 to −3.5 V. The h_ss used for depicting the topographic images are 0.7, 1.0, 1.7, and 1.8 nm for the images with V_{max} = −2.0, −2.5, −3.0, and −3.5 V, respectively. (d) (top) Topographic and (bottom) current C-AFM images observed after set switching with V_{max} = +3.0 V (following the first reset switching with V_{max} = −3.5 V). The broken white circles in the C-AFM images mark the peripheries of the contact positions of the C-AFM tips in the $I-V$ measurements, where a high-resistance core was formed after the abrupt reset. The scan area of the C-AFM images is 200 × 200 nm^2, and a reading voltage of −1.0 V was applied to acquire the current images.

S3. The mechanical contact radius between the tip and film was estimated as 1.2 nm from the Hertz model,[29] but the C-AFM images suggested that the effective electrical contact radius in the $I-V$ measurements was increased to 27 nm (which corresponds to the radius of the 0.3 nm deformation) due to the field spreading and water meniscus formation.[30,31] Conductive regions became observable in the current images under I_c ≥1.0 μA, where a large decrease in the switched resistance was demonstrated in the $I-V$ characteristics. The size change of the conductive region, which has been widely assumed in previous studies,[4,5,7,8,11,14,15] was observed between I_c = 1.0 and 2.0 μA (from 5 to 14 nm in radius), while a less sensitive I_c dependence was shown for the switched resistance (Figure 1c). From 20 times $I-V$ measurements of the switching at separated positions, the average values of the switched resistance (read at +0.1 V) and its standard deviations were determined as 170 kΩ and 56 kΩ at I_c = 1.0 μA and 97 kΩ and 25 kΩ at I_c = 2.0 μA, respectively. Therefore, the I_c dependence of the switched resistance was still significant in the I_c range of 1.0−2.0 μA, even though the sensitivity was much reduced. The structural deformation after the switching was still small at I_c = 2.0 μA, and the switching at I_c = 2.0 μA caused no detectable topographic deformation in a-TaO_x when it was conducted with negative voltages (Figure S4). A further increase in I_c did not cause a size increase in the conductive region but resulted in shape disorder. At I_c ≥ 10 μA, the height of the topographic deformation of a-TaO_x was increased to 1.0 nm (at the maximum part), and the conductive regions were divided into multiple areas in the current images. Note that the relatively large upward deformation of a-TaO_x may be suppressed in a practical device with a top electrode layer due to internal stresses from the layer and may result in a partly different behavior of ion migration. Accompanying the path division for I_c ≥ 10 μA, the sign of the I_c dependence of the switched resistance was reversed in the $I-V$ characteristics (top panel of Figure 1c), indicating the occurrence of an "over-set (over-forming)" phenomenon[32] in the a-TaO_x thin film. In previous studies, the occurrence of similar relatively large, nanoscale upward deformation of a switching material has been observed in binary-type forming switching of a-TaO_x thin films based on the probe microscopy measurements,[18,19] while no observable structural deformation has generally been caused in forming switching of other materials.[24,27] The structural deformation of a-TaO_x observed in Figures 1d and S3 is therefore attributable to the high cation mobility of a-TaO_x reported in the previous studies,[18,19] as discussed later.

2.3. C-AFM Observation of Voltage-Dependent Analog Reset. Figure 2a shows the V_{max} dependence of the reset switching characteristics of an a-TaO_x thin film, measured by C-AFM after the initial set switching operations. In the measurements, positive DC voltages were applied to the film with various V_{maxs} of +1.0−+5.0 V after inducing the initial set switching at I_c = 2.0 μA, by which a robust conduction path can be formed without large structural deformation of a-TaO_x (middle panels of Figure 1d). Gradual reset switching and significant V_{max} dependence of the switched resistance were observed in the $I-V$ characteristics with V_{max} = +1.5−+2.5 V. Therefore, the (2) V_{max}-dependent analog reset phenomenon[3,4,6,8,13] was demonstrated in this V_{max} range with input powers of 0.2−0.4 mW, which are equivalent to those in practical devices.[3,10,28] Through voltage application with V_{max}

https://doi.org/10.1021/acsami.2c21568
ACS Appl. Mater. Interfaces 2023, 15, 16842−16852

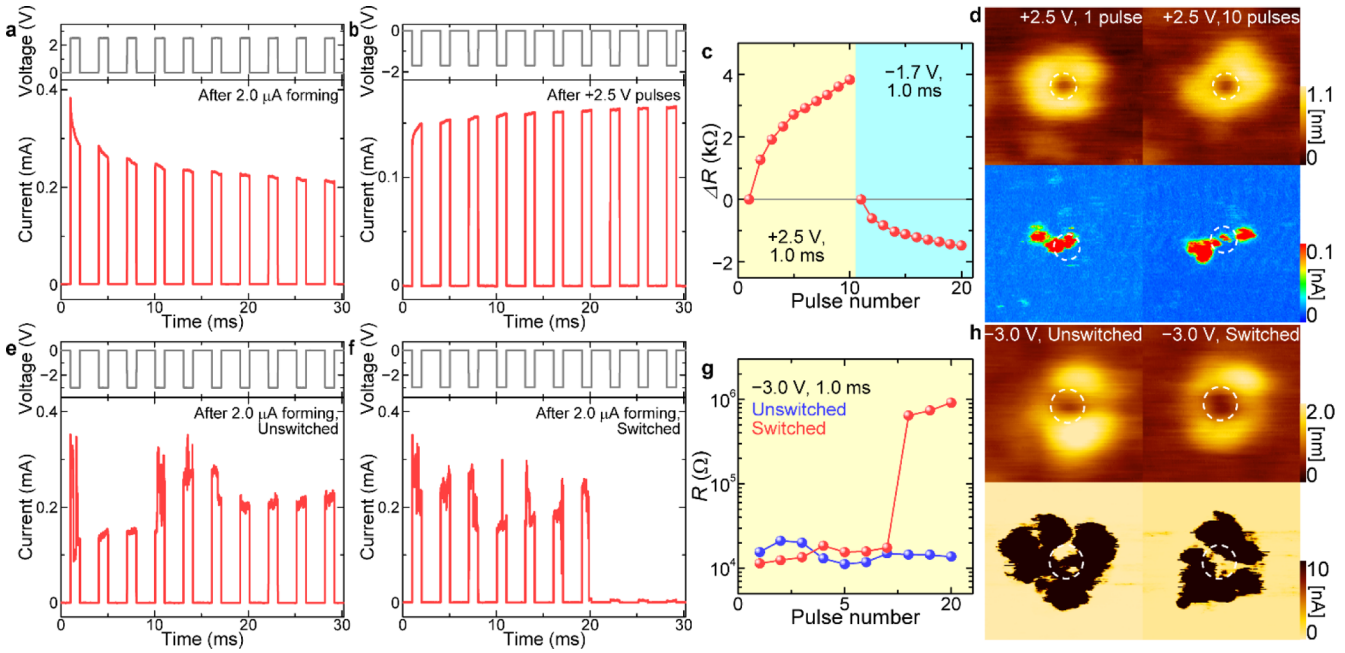

Figure 4. $I-t$ characteristics of an a-TaO_x thin film measured by applying pulsed voltage stresses of (a) +2.5 V after a forming operation at I_c = 2.0 μA and (b) −1.7 V after the 10-time reset operation induced by pulsed voltages of +2.5 V. (c) Differential resistances (ΔRs) determined for each voltage pulse shown in (a) and (b), from which the resistances for the first pulses are subtracted. (d) (top) Topographic and (bottom) current C-AFM images of the a-TaO_x thin film observed directly after the one-time application and 10-time application of pulsed voltages of +2.5 V. $I-t$ characteristics of an a-TaO_x thin film measured by applying pulsed voltage stresses of −3.0 V after a forming operation at I_c = 2.0 μA, where the sudden resistance increase was (e) not observed and (f) observed. (g) Resistances determined for each voltage pulse shown in (e) and (f). (h) (top) Topographic and (bottom) current C-AFM images of the a-TaO_x thin film observed directly after 10-time application of pulsed voltages of −3.0 V for the areas where the sudden reset was not observed and was observed. The voltages applied in the $I-t$ measurements are shown in the top panels. The broken white circles in the C-AFM images mark the peripheries of the contact positions of the C-AFM tips in the $I-t$ measurements. The scan area of the C-AFM images is 200 × 200 nm^2, and a reading voltage of −1.0 V was applied to acquire the current images.

≤ +1.5 V, the a-TaO_x thin film first formed a volcano-like structure with a maximum height of 1.1 nm in the conductive region (left panels of Figures 2c and S5 for the height information in this type of switching), which suggests the occurrence of upward migration of the internal cations (Ta^{5+} and Ta^{4+}).[18,19] However, this ion migration did not cause significant reset switching in the a-TaO_x film, as indicated by the $I-V$ characteristics and current image. At V_{max} = +1.5−+2.5 V, where the analog reset was demonstrated, instead, gradual volume increases of a-TaO_x were observed in the conductive regions. At +2.5 V, where the analog reset was completed in the $I-V$ characteristics, a symmetric mound with a height of 1.2 nm was formed in the topographic structure of a-TaO_x, and the conductive area almost disappeared in the current image. The mound-like structure is indicative of the occurrence of mass supply from the tip side, which is generally caused by anodic oxidation of the film.[30] By subsequently applying negative voltages with V_{max} = −1.7 V after the reset, very stable cycling of the analog resistive switching was demonstrated in the film (Figure 2b), showing switching behavior similar to that of a-TaO_x-based memristive devices.[3,4,8] The volume of a-TaO_x decreased again after the set switching at −1.7 V, and a conductive region reappeared in the current image (Figure 2d). At V_{max} > +2.5 V (right panel of Figure 2a), in contrast, the switched resistance decreased from that at V_{max} = +2.5 V, with the occurrence of spiking currents during voltage sweeping. Such behavior has also been observed in a-TaO_x device structures as the "over-reset" or "reset failure" phenomenon.[8] Interestingly, we observed that characteristic dendrite structures were formed in the film after over-reset at V_{max} = +5.0 V over a long distance of 450 nm (Figures 2c and S5).

2.4. C-AFM Observation of Stochastic Switching. The C-AFM measurements also demonstrated that the continuity and stochasticity of the resistive switching can be drastically changed in a-TaO_x depending on the polarity of the applied voltages. Figure 3a shows the DC $I-V$ characteristics of an a-TaO_x thin film measured under negative voltages with V_{max} = −2.0 to −3.5 V by C-AFM after inducing the initial set switching at I_c = 2.0 μA. The characteristics of a subsequent set switching with V_{max} = +3.0 V (measured after the −3.5 V reset) are also shown in the figure. Unlike the analog-type switching observed under the voltage polarity sequence of +2.5 → −1.7 V (Figure 2b), very abrupt resistive switching was induced under the sequence of −3.5 → +3.0 V with the defined switching voltages of −3.2 V and +2.5 V, and this type of $I-V$ characteristic is also typical in a-TaO_x-based resistive switching devices.[3,5,6,13] In this voltage sweeping sequence, structural depression was first caused at −1.5 V by the downward migration of Ta^{5+} and Ta^{4+} in the conduction path (Figure S6), while the deformation did not cause significant reset switching. The reset switching started to be induced after a small resistance jump at −1.8 V (Figure 3a) and then progressed with the generation of spiking current noise. From V_{max} = −2.0 to −3.0 V, gradual expansion of the conductive areas was observed in the current images (Figure 3c) despite the progress of the reset switching in the $I-V$ characteristics. After a large resistance jump was caused at −3.2 V, remarkably, structural coalescence was observed in the film with the occurrence of nanoparticle structures with a maximum height

https://doi.org/10.1021/acsami.2c21568
ACS Appl. Mater. Interfaces 2023, 15, 16842−16852

of 2.0 nm (top right panel of Figure 3c), suggesting a change in the chemical bonding states of a-TaO_x. In addition, a unique core−shell structure was formed in the resistance distributions of a-TaO_x after the abrupt reset switching (bottom right panel of Figure 3c). In previous studies on resistive switching oxides, the formation of a core−shell structure has been considered for a material after set switching,[33,34] and lower resistance has been supposed for the central core part. However, in our measurements, the presence of a reverse-type structure with a higher-resistance core was found in the films after reset switching. After the subsequent set switching at +2.5 V, the region of the higher-resistance core was invaded by the surrounding conductive shell with the occurrence of upward topographic migration (Figure 3d). Cycling $I-V$ measurements demonstrated that this type of switching has large distributions in the switching voltages and switched resistances (Figure 3b), which suggests stochasticity of its occurrence. Moreover, the measurements indicated that the structural coalescence of a-TaO_x progressively increased with cycling of the stochastic-type switching (Figure S7).

2.5. C-AFM Observation of Time-Dependent Analog Switching. In the a-TaO_x thin films, continuous resistance changes induced by multiple voltage applications [i.e., (3) voltage-application-time-dependent analog switching][4,7,8] were observed under the analog type of voltage polarity sequence (positive forming → positive reset → negative set). As shown in Figure 4a−c, systematic changes in the resistance were demonstrated in an a-TaO_x film with application of sequential pulsed voltages of +2.5 or −1.7 V with a duration of 1.0 ms (after the initial set at I_c = 2.0 μA). In these operations, a volcano-like structure was formed after the first voltage stress of +2.5 V (top left panel of Figure 4d) by the upward migration of Ta^{5+} and Ta^{4+}. However, the topographic images did not significantly change further with the progress of analog switching, whereas the resistance levels were altered in the current images (Figures 4d and S8). In this type of analog switching, the resistance of a-TaO_x also showed a dependence on the time interval of the applied voltages (Figure S9), which supports the second-order memristor characteristics of a-TaO_x.[7]

Under the stochastic type of voltage polarity sequence (positive forming → negative reset → positive set), instead, continuous resistance changes were not induced for a-TaO_x by pulsed voltage application, but the temporal stochasticity of the switching was confirmed in the measurements. Figure 4e,f shows the $I-t$ characteristics of an a-TaO_x thin film measured by applying pulsed voltage stresses of −3.0 V (after the initial set operations at I_c = 2.0 μA). The measurements demonstrated that the multiple voltage applications stochastically induce an abrupt reset of a-TaO_x from approximately 10^4 Ω to 10^6 Ω (Figure 4g) within the first 10 voltage stresses. Periodic spiking currents with a high frequency of >0.7 MHz were also observed in the $I-t$ characteristics as noise currents during the single pulsed voltage (Figure S10). After the multiple voltage applications, structural coalescence and formation of the core−shell structures were caused in a-TaO_x (Figure 4h), but some conductive areas remained in the higher-resistance core when the abrupt reset switching was stochastically not induced (left panels in Figure 4h).

In addition, our C-AFM measurements revealed that the very high switching speed of a-TaO_x, which has been reported in device structures with a switching time of down to <1.0 ns,[3,28,35] can be obtained in the stochastic type. Figure 5a,c shows the $I-t$ characteristics of an a-TaO_x film measured using an oscilloscope-based C-AFM setup for high-speed measurements (Figure S11). Under the analog-type reset operation (a pulsed voltage stress of +2.5 V after the initial set at I_c = 2.0 μA), the film did not show significant reset switching within the duration of 100 ns in the $I-t$ characteristics or current image (Figure 5a,b), suggesting the limited switching speed of this type. This operation structurally caused upward deformation of the conductive region in a-TaO_x, and the deformed area was smaller than that after 1.0−10 ms (Figure 4d). By applying a pulsed voltage stress of −3.0 V (i.e., the stochastic-type reset operation), in contrast, fast reset switching with a switching time of <100 ns was demonstrated in the $I-t$ characteristics and current image (Figure 5c,d), while this switching was cancelled out as the spiking noise on longer time scales (Figures 3a and 4e). After the reset switching, a 0.2 nm depth topographic depression was formed at the tip−contact position in the conductive region (white crosses, as shown in Figure 5d). The observed topographic changes strongly suggested that the fast reset switching at −3.0 V was produced by downward migration of the Ta^{5+} and Ta^{4+} ions, and

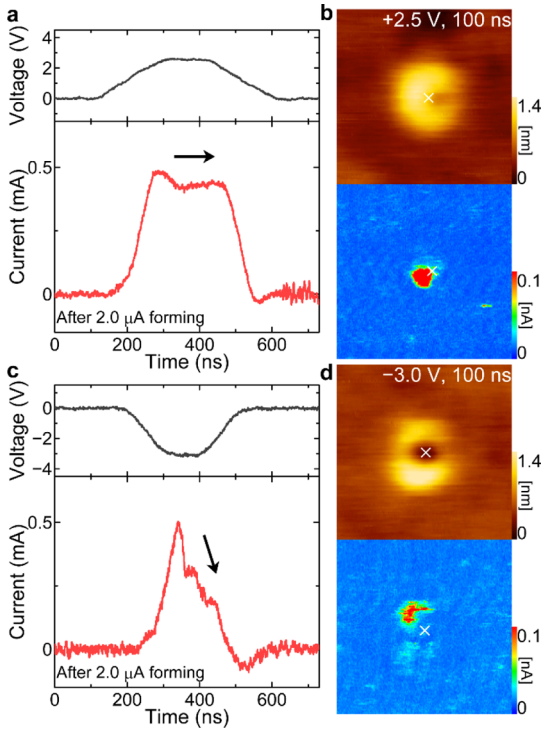

Figure 5. (a) $I-t$ characteristics of an a-TaO_x thin film measured by applying a pulsed voltage stress of +2.5 V with a duration of 100 ns (after the initial set at I_c = 2.0 μA). (b) (top) Topographic and (bottom) current C-AFM images of the a-TaO_x thin film observed directly after the voltage application shown in (a). (c) $I-t$ characteristics of an a-TaO_x thin film measured by applying a pulsed voltage stress of −3.0 V with a duration of 100 ns (after the initial set at I_c = 2.0 μA). (d) (top) Topographic and (bottom) current C-AFM images of the a-TaO_x thin film observed directly after the voltage application shown in (c). The voltages applied in the $I-t$ measurements are shown in the top panels. The white crosses in the C-AFM images mark the contact positions of the C-AFM tips in the $I-t$ measurements. The scan area of the C-AFM images is 200 × 200 nm^2, and a reading voltage of −1.0 V was applied to acquire the current images. The maximum current levels in the current-mapping observations (for the red regions of the current images) were 4.0 nA in (b) and 0.6 nA in (d).

https://doi.org/10.1021/acsami.2c21568
ACS Appl. Mater. Interfaces 2023, 15, 16842−16852

disconnection of the conduction path was preferentially caused by the downward migration because of the large electrode area difference between the top and bottom interfaces (Figure S12). The 0.2 nm depression observed after the voltage application time of 100 ns roughly gives a drift velocity of 0.2 cm/s for Ta^{5+} and Ta^{4+} at the applied field of 5.3 MV/cm. This value is in reasonable agreement with the typical ion drift velocity of a metal oxide with a small activation energy[36] and may explain the intrinsically high switching speed of a-TaO_x.

2.6. Switching Mechanisms. In discussing the physical mechanisms of the observed switching, we should consider the fact that a-TaO_x has a particularly sensitive dependence of the resistivity on the oxygen composition for $x = 2.0-2.5$[37−39] as a binary amorphous metal oxide. This feature has been explained based on the absence of any stable suboxide phase in this composition range[37] due to the particularly simple thermodynamic diagrams of amorphous and crystalline TaO_x,[37,40,41] which include only two stable phases of Ta and $TaO_{2.5}$. Regarding the driving factors of the ion migration, mass fluxes previously considered for binary-type resistive switching phenomena,[42−45] such as those driven by electric drift (J_d in Figure 6), compositional (Fick) diffusion, and thermal (Soret)

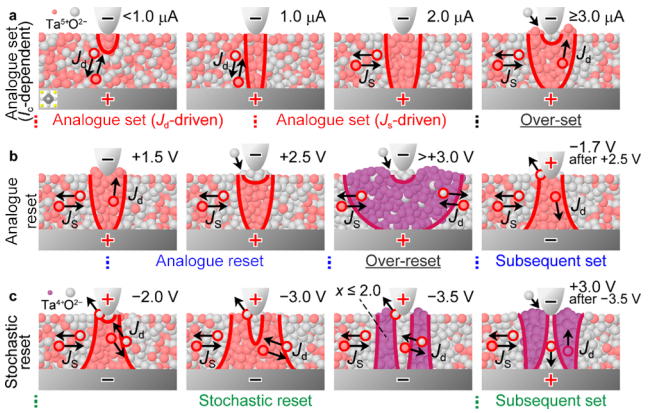

Figure 6. Schematic illustrations of the possible mechanisms of the ion migration in the a-TaO_x thin films under the (a) current-dependent analog set, (b) voltage-dependent analog reset, and (c) stochastic reset phenomena observed in our C-AFM measurements. J_d and J_S in the illustrations denote the mass fluxes of the ions driven by electric drift and Soret diffusion, respectively. The Ta^{5+}, Ta^{4+}, and O^{2-} ions drawn in the ratios of their Shannon ionic radii[48] are shown at the upper left of (a) and (c). The conductive regions before and after the segregation of a-TaO_2 are drawn as the internal areas of the red solid lines with the pink balls (Ta^{5+}) and internal areas of the magenta solid lines with the purple balls (Ta^{4+}), respectively. Note that the composition ratios of the tantalum ions to the oxide ions in the conductive regions are increased from the actual values for clarity. Also, the aspect ratio of the a-TaO_x thin films and relative heights of the structural deformations on the surfaces are modified in the illustrations.

diffusion (J_S in Figure 6), are also applicable. In our a-TaO_x thin films, however, the influence of compositional diffusion was suggested to become significant on a time scale of over 200 ms (Figure S9). We confirmed that no detectable chemical contamination was caused between the a-TaO_x thin films and Rh-coated tips in the C-AFM measurements (Figures S13−S15), and the Ta^{5+}, Ta^{4+}, and O^{2-} ions have a lateral migration distance of over 250 nm in the resistive switching (Figures S16 and S17). Note that the ion migration discussed here refers to both migration of the interstitial ions and vacancy-mediated migration of the ions in the host structures, while the interstitial/vacancy-mediated mechanism is considered relatively dominant for the tantalum/oxide ions,[18,44,46] respectively. Also, we mention that the lateral ion-migration distance observed in our C-AFM experiments is in good agreement with that previously observed for resistive switching of a-TaO_x (6.0 nm) thin films by X-ray absorption spectromicroscopy.[47] Based on the above facts and the observed C-AFM images, we suggest the possible mechanisms of the observed resistive switching as follows.

In the (1) I_c-dependent analog set phenomenon (Figures 1c,d and S3), the C-AFM images suggested that a-TaO_x with reduced resistivity was partially formed at the top interface of the film at $I_c < 1.0$ μA due to the vertical electric drift and accumulation of the Ta^{5+} ions, and a penetration path was formed at $I_c = 1.0$ μA by the increased amount of conductive a-TaO_x (Figure 6a). Under the accumulation, the x in a-TaO_x at the top interface decreases from the initial value (around 2.46), and the sensitive I_c dependence of the switched resistance (bottom panel of Figure 1c) is considered to be due to the steep oxygen composition dependence of the resistivity. The absence of a conductive spot in the current images for $I_c < 1.0$ μA (Figures 1d and S3) supports this assumption since the partially reduced regions will be reoxidized from the top surfaces in the subsequent scanning measurements. The rapid increase in the conductive areas observed at $I_c = 1.0-2.0$ μA (Figure 1d) suggested that lateral migration of Ta^{5+} was caused in this I_c range by Soret diffusion[42−45] toward the thin (high-current-density) conduction path formed at 1.0 μA (second left panels of Figure 1d). As mentioned above, the radius of the robust conduction path that formed at $I_c = 2.0$ μA was 14 nm in the current image (Figure 1d), while the structural radius observed in the topographic image was 35 nm. In recent experiments for a-TaO_x thin films based on transmission electron microscopy[44] and X-ray photoemission electron microscopy,[49] the radius of a conduction path involved in the resistive switching has been shown to be 33 nm and 25−45 nm, respectively, from the local increases in the tantalum ion composition. Thus, if we assume that the structural deformation of a-TaO_x observed at $I_c = 2.0$ μA was mainly caused by the vertical and lateral accumulation of Ta^{5+} ions, a good agreement with the previous microscopy observations can be seen in the structural size of the conduction path for the C-AFM observations of this study. As discussed in Analyses of the Chemical Compositions section of Supporting Information, the oxygen composition x in the conduction path after the set switching at $I_c = 1.0-2.0$ μA was suggested to be close to (but larger than) 2.0 for the present a-TaO_x thin films. This composition value is also well consistent with the chemical composition of the conduction path in a-TaO_x ($x = 2.0 \pm 0.1$) determined in the recent observations by X-ray photoemission electron microscopy.[49] The relatively large topographic deformation observed at $I_c \geq 3.0$ μA (Figures 1d and S3) indicated that increased vertical migration of tantalum ions (Ta^{5+} and Ta^{4+}) was caused in the conduction paths under these I_cs due to the increased transport number of tantalum ions induced by the reduction of a-TaO_x.[19,45] The migration of tantalum ions, however, will not cause a further decrease in the switched resistance, as observed in the $I-V$ characteristics (Figure 1c). The path spreading observed in the current images with $I_c \geq 10$ μA (Figures 1d and S3) suggested that the influences of the electrochemical oxidation became significant at the top interfaces under these current levels (right

https://doi.org/10.1021/acsami.2c21568
ACS Appl. Mater. Interfaces 2023, 15, 16842−16852

illustration in Figure 6a), and the over-set phenomenon was caused by the increased resistivity of a-TaO_x. The increased contributions from the electrochemical oxidation at the larger I_cs are directly predictable from the increases in the flowing currents because the rate of the anodic oxidation (a-TaO_x + $y$$OH^-$ + $y$$h^+$ → a-TaO_{x+y} + $y$$H^+$ + ye^-) is in principle dependent on or proportional to the oxidation current.[30,31]

The volume increases of a-TaO_x observed in the (2) V_{max}-dependent analog reset phenomenon (+1.5 to +2.5 V in Figures 2c and S5) suggested that the resistance increases in this type of switching were produced by the electrochemical oxidation of a-TaO_x (second left illustration in Figure 6b). The oxidation from air (replacement of an oxygen reservoir layer in a practical device),[5,10,28] which was suggested for $I_c \geq 10$ μA in the over-set, should also progress in this reset switching at approximately 150 μA and will steeply increase the resistivity of a-TaO_x at the interface. The reversibility of the structural changes (Figures 2c,d and S7) and stability of the cycling characteristics (Figure 2b) indicated that the redox reactions involved in this switching are highly continuous and reversible (Figure 6b), possibly due to the low probability of phase separation in a-TaO_x for $2.0 < x < 2.5$. The dendritic structures observed after the over-reset at V_{max} = +5.0 V (Figures 2a,c and S5) are known as typical structures of thin-film ionic conductors after application of high electric fields, by which ion migration was also induced in the in-plane direction.[50] Therefore, these structures strongly suggest that the over-reset characteristics of a-TaO_x originate in the lateral electric drift of the Ta^{5+} ions caused by the excessive voltage application (J_d in the second right illustration of Figure 6b). The (3) time-dependent analog switching phenomenon observed with multiple pulsed voltage applications (Figure 4a,b) is also considered based on the electrochemical redox reactions under the analog-mode voltage polarity sequence (+2.5 → −1.7 V) (second left and right illustrations in Figure 6b). The monotonic time dependence of the resistance consistently suggested the dominant role of the electrochemical redox reactions because the extent in principle changes with the amount of injected charge (i.e., the time integral of the current).

In the stochastic-type reset under negative voltages (Figure 3a), in contrast, the O^{2-} ions will accumulate at the top interface due to the electric drift, and reduction reactions with air will be caused (Figure 6c). Under these conditions, competing resistance increases and decreases will be simultaneously caused at the top interface of the a-TaO_x film, which may explain the generation of spiking currents (Figure 3a). With the progress of voltage application, the total oxygen content in a-TaO_x will be progressively decreased by the reduction reactions, as supported by the expansion of the conductive areas for V_{max} = −2.0 to −3.0 V (Figure 3c). This suggests that the structural coalescence observed in a-TaO_x (−3.5 V in Figure 3c) was compositionally caused by oxygen reduction through segregation of a different chemical phase with $x < 2.46$. The oxygen composition x in the coalesced nanoparticle region was shown to be approximately or slightly less than 2.0 by Auger electron spectroscopy (AES, Figure S13). Based on the analyzed compositions and phase configuration of the a-TaO_x system, the formation of a-TaO_2, which is a metastable metallic phase with a relatively high thermodynamic stability,[18,41] in stochastic-type reset switching was suggested. When this formation is considered, the origin of the switching stochasticity is attributable to the metastability of a-TaO_2, due to which segregation will occasionally be induced in voltage sweeping (Figure 3a) and multiple voltage applications (Figure 4e,f). The C-AFM images after switching (Figure 3c) indicated that the abrupt resistance increase in the stochastic reset was caused by the formation of a high-resistance core structure. The possibility of a-TaO_2 segregation suggests that the abrupt formation of the high-resistance core results from rapid radial exchange of Ta^{5+}/Ta^{4+} and O^{2-} ions between the core and shell regions, caused by compositional segregation (second right illustration in Figure 6c). The set switching after the stochastic reset (Figure 3d and right illustration in Figure 6c), in contrast, will be produced by the electric drift of Ta^{5+} and Ta^{4+} from the shell part since the coalesced a-TaO_2 is not largely decomposed in the switching cycles, as observed in Figure S7.

3. CONCLUSIONS

The physical mechanisms of the analog resistive switching phenomena were directly visualized in a-TaO_x using atomically flat thin films. Our results based on C-AFM indicate that a stable analog switching phenomenon can be induced in a-TaO_x by causing the reversible redox reactions, which will continuously progress in a composition range of $2.0 < x < 2.5$. A way of toggling the switching stochasticity was also demonstrated in the C-AFM measurements, possibly based on the compositional segregation of heterogeneous a-TaO_2. These results suggest that a steep oxygen composition dependence of the resistivity and suppression of phase segregation, which were provided in a-TaO_x in this study, are key factors for analog switching operations of an amorphous metal oxide, while phase segregation will play a critical role in stochastic-type switching. We believe that the insights from this study open the possibility of directly controlling the switching functions of a metal oxide for applications in neuromorphic computing (including artificial synapses and stochastic switching elements) and offer opportunities to explore new hardware-driven neuromorphic functionalities.

4. EXPERIMENTAL SECTION

4.1. Film Preparation. Atomically flat thin films of a-TaO_x were deposited by the PLD method on Nb:STO (001) substrates with a Nb concentration of 0.05 wt.% (supplied by Shinkosha Co., Ltd.). On the Nb:STO (001) substrates, step-and-terrace surfaces with single-unit-cell-height (0.3905 nm) steps were formed by buffered hydrofluoric acid etching prior to deposition. The meandering patterns of the substrate steps, which were formed through etching, also served as position marks in the C-AFM measurements. Film deposition by PLD was conducted at room temperature (without substrate heating) and a P_{O2} of 10^{-4}–10^{1} Pa, and a sintered ceramic disc of Ta_2O_5 (99.9%, Kojundo Chemical Lab. Co., Ltd.) was used as the target. Focused third harmonics of a Nd:YAG laser (wavelength = 355 nm) were used as the ablation light source for PLD, and the power and repetition frequency were set as 15 mJ and 10 Hz, respectively. Among the a-TaO_x thin films, 5.7 nm thick films deposited at P_{O2} = 5.0 × 10^{-4} Pa were used for the C-AFM measurements.

4.2. Film Characterization. The thickness and mass density of the a-TaO_x thin films were determined by X-ray reflectometry using an X-ray diffractometer (ATX-G, Rigaku Co., Ltd.). Characterizations of the atomic structures and film porosity were performed via transmission electron microscopy on a JEM-ARM200F microscope (JEOL Co., Ltd.) for a-TaO_x (200 nm)/SiO_2/Si thin films patterned by focused ion beam milling with an FB-2000A system (Hitachi). The resistivity of a-TaO_x was measured by the DC four-point probe method (in the van der Pauw electrode configuration) with a source

https://doi.org/10.1021/acsami.2c21568
ACS Appl. Mater. Interfaces 2023, 15, 16842−16852

measurement unit (Keithley 2450) for a-TaO_x (50 nm)/glass (CORNINGEAGLE XG) thin films. The chemical compositions of the a-TaO_x (5.7 nm)/Nb:STO (001) thin films and Rh-coated C-AFM probes were analyzed by X-ray photoelectron spectroscopy with a photoelectron spectrometer (JEOL Co., Ltd., JPS-9200) and AES with an Auger electron spectrometer equipped with a field-emission scanning electron microscope (JEOL Co., Ltd., JAMP-9500F).

4.3. C-AFM Measurements. C-AFM measurements for the a-TaO_x/Nb:STO (001) thin films were conducted with a system consisting of a scanning probe microscope (Nanocute, Hitachi High-Tech Co., Ltd.) and a semiconductor parameter analyzer (B1500A, Keysight Co., Ltd.) equipped with a waveform generator/fast measurement unit (B1530A, Keysight Co., Ltd.). In the C-AFM measurements, DC $I-V$ and pulsed $I-t$ characteristics with a time resolution of >1.0 μs were measured using the B1500A analyzer, and current-mapping images were acquired using the C-AFM module of the Nanocute and a current preamplifier (LI-76, NF Co., Ltd.). Pulsed $I-t$ measurements with a time resolution of <1.0 μs were conducted in a different C-AFM setup, as shown in Figure S11. Pulsed voltage stresses were applied from a pulse generator (81110A, Keysight Co., Ltd.) in the setup, and currents were derived from the voltage readings of an oscilloscope (DLM2022, Yokogawa Co., Ltd.). Current fluctuations due to contact area variations of the C-AFM probe[51] were not significantly observed in the C-AFM $I-V$ measurements, owing to the uniformity of the electrical contact between the atomically flat a-TaO_x films and conductive probes. Irreversible breakdown of the materials, which is known as a serious problem in C-AFM measurement of a resistive switching phenomenon, was also significantly suppressed and hardly observed in the voltage range of the measurements because of the uniform (not locally focused) field application expected for the tip/film contacts (as indicated by the uniform structural deformation shown in Figure 1d).

To investigate the analog resistive switching phenomena by C-AFM, we should note that analog switching of an a-TaO_x device has been demonstrated by fabricating a multilayer structure with a layer for oxygen exchange (so-called "oxygen reservoir"), such as an a-TaO_x layer with a different oxygen composition[3,4,6,7,10] and an interface layer with a reactive electrode (Ta and Ti),[5,6,8,13] in almost all cases. To obtain this effect in the C-AFM technique, we conducted measurements in air, in which oxide ions can be readily supplied from and exposed to the gas phase and water meniscus. The relative humidity in the ambient air was kept at 30−40% during the C-AFM measurements. We confirmed that the switching properties and topographic structures of the a-TaO_x thin films are not significantly influenced by humidity variations within this range. In addition, when the electrical contact radius in the C-AFM measurements is assumed to be 27 nm, the resistivity of the Nb:STO substrate with a Nb doping level of 0.05 wt.% (10^{-1} Ω cm) gives a spreading resistance R_{spread} of 10 kΩ,[52] which is in series with the a-TaO_x thin film. This R_{spread} is comparable to the resistance of the a-TaO_x thin films in the low resistance state and is in a range effective as a load resistance element for suppressing the excessive transient currents in the circuit,[53] which has been widely employed in practical device structures to improve the effectiveness of I_c control.

As conductive probes, Si cantilevers coated with 30 nm thick layers of Rh (supplied by Hitachi High-Tech Co., Ltd.) were used in the C-AFM measurements. The contact force was set as 8 nN during the $I-V$, $I-t$, and scanning measurements to suppress the contributions from the flexoelectricity, heating, and structural modification of the measured films, which typically become significant under a contact force of >100 nN.[22] The weak contact force and tip curvature radius of 25 nm ensured a uniform electrical contact area of 2300 nm^2 in the $I-V$ and $I-t$ measurements (as observed in Figure 1d). This defined contact area is well comparable to the typical electrode areas of practical resistive switching devices,[54] where sharp plug or nanoparticle structures are often fabricated on the electrodes to confine the resistive switching spot. These experimental features therefore suggest that the operation conditions of practical resistive switching devices of a-TaO_x were reasonably reproduced in the C-AFM measurements conducted in this study in the many aspects of the electrical input levels, structural dimensions (areas and thicknesses), and multilayer functions (oxygen reservoir and load resistance), and the observed resistive switching can provide phenomenal examples of the device properties.

■ ASSOCIATED CONTENT

Supporting Information

The Supporting Information is available free of charge at https://pubs.acs.org/doi/10.1021/acsami.2c21568.

Details of the PLD fabrication of atomically flat a-TaO_x thin films; X-ray photoelectron spectrum for an atomically flat a-TaO_x thin film in the initial state; detailed set of C-AFM images of an a-TaO_x thin film after the current-dependent analog set; C-AFM images of an a-TaO_x thin film after initial set switching under negative voltage; three-dimensional drawings of the C-AFM images of an a-TaO_x thin film after the voltage-dependent analog- and over-reset phenomena; C-AFM images of an a-TaO_x thin film observed at V_{max} = −1.5 V before the stochastic reset phenomenon; C-AFM images of an a-TaO_x thin film observed after cycling measurements of the analog and stochastic resistive switching; three-dimensional drawings of C-AFM images of an a-TaO_x thin film after the time-dependent analog switching operations; C-AFM results on interval time dependence of the time-dependent analog switching characteristics; results of power spectral density analysis for the current spiking phenomenon in the stochastic-type switching; description of the measurement circuit used for the high-speed electrical measurements by C-AFM; possible ion distributions in a-TaO_x thin films under the short pulse reset switching operations; results of AES analysis for an a-TaO_x thin film after switching operations by C-AFM; results of AES analysis for Rh-coated C-AFM probes after switching operations; C-AFM images of bare Nb:STO (001) surfaces observed after DC $I-V$ measurements; AFM images of structural changes observed in the periphery region of the conduction path in an a-TaO_x thin film; and AFM images of changes in the step-and-terrace structures on a-TaO_x observed after the analog switching operations (PDF)

■ AUTHOR INFORMATION

Corresponding Author

Atsushi Tsurumaki-Fukuchi − *Faculty of Information Science and Technology, Hokkaido University, Sapporo 060-0814, Japan;* orcid.org/0000-0003-2529-8897; Email: a.fukuchi@ist.hokudai.ac.jp

Authors

Takayoshi Katase − *Laboratory for Materials and Structures, Institute of Innovative Research, Tokyo Institute of Technology, Yokohama 226-8503, Japan;* orcid.org/0000-0002-2593-7487

Hiromichi Ohta − *Research Institute for Electronic Science, Hokkaido University, Sapporo 001-0020, Japan;* orcid.org/0000-0001-7013-0343

Masashi Arita − *Faculty of Information Science and Technology, Hokkaido University, Sapporo 060-0814, Japan*

Yasuo Takahashi − *Faculty of Information Science and Technology, Hokkaido University, Sapporo 060-0814, Japan*

https://doi.org/10.1021/acsami.2c21568
ACS Appl. Mater. Interfaces 2023, 15, 16842−16852

Complete contact information is available at:
https://pubs.acs.org/10.1021/acsami.2c21568

Author Contributions

A.T.-F. conceived this project and designed the experiments. T.K. and H.O. fabricated the atomically flat thin films of a-TaO_x and characterized them. M.A. and Y.T. interpreted the results on resistive switching phenomena and supervised the group. A.T.-F. conducted the C-AFM and AES measurements and wrote the manuscript. All the authors contributed to the discussion of the experimental results and preparation of the manuscript at all stages.

Notes

The authors declare no competing financial interest.

■ ACKNOWLEDGMENTS

This work was financially supported by the Japan Society for the Promotion of Science (JSPS, KAKENHI nos. 19K04484 and 19H05791) organized by the Ministry of Education, Culture, Sports, Science, and Technology (MEXT), Japan. Part of this work was conducted under the Nanotechnology Platform by MEXT at the Laboratory of XPS analysis, Hokkaido University and Collaborative Research Projects of Laboratory for Materials and Structures, Institute of Innovative Research, Tokyo Institute of Technology.

■ REFERENCES

(1) Yu, S.; Wu, Y.; Jeyasingh, R.; Kuzum, D.; Wong, H. S. P. An Electronic Synapse Device Based on Metal Oxide Resistive Switching Memory for Neuromorphic Computation. *IEEE Trans. Electron Devices* **2011**, *58*, 2729−2737.

(2) Wang, Z. Q.; Xu, H. Y.; Li, X. H.; Yu, H.; Liu, Y. C.; Zhu, X. J. Synaptic Learning and Memory Functions Achieved Using Oxygen Ion Migration/Diffusion in an Amorphous InGaZnO Memristor. *Adv. Funct. Mater.* **2012**, *22*, 2759−2765.

(3) Lee, S. R.; Kim, Y.-B.; Chang, M.; Kim, K. M.; Lee, C. B.; Hur, J. H.; Park, G.-S.; Lee, D.; Lee, M.-J.; Kim, C. J.; Chung, U.-I.; Yoo, I.-K.; Kim, K. Multi-Level Switching of Triple-Layered TaO_x RRAM with Excellent Reliability for Storage Class Memory. In *2012 Symposium on VLSI Technology (VLSIT); Hawaii, USA, June 12−14*; IEEE, 2012; pp 71−72. DOI: 10.1109/VLSIT.2012.6242466.

(4) Kim, S.; Choi, S.; Lee, J.; Lu, W. D. Tuning Resistive Switching Characteristics of Tantalum Oxide Memristors through Si Doping. *ACS Nano* **2014**, *8*, 10262−10269.

(5) Prakash, A.; Park, J.; Song, J.; Woo, J.; Cha, E.-J.; Hwang, Y. Demonstration of Low Power 3-Bit Multilevel Cell Characteristics in a TaO_x-Based RRAM by Stack Engineering. *IEEE Electron Device Lett.* **2015**, *36*, 32−34.

(6) Kim, K. M.; Lee, S. R.; Kim, S.; Chang, M.; Hwang, C. S. Self-Limited Switching in Ta_2O_5/TaO_x Memristors Exhibiting Uniform Multilevel Changes in Resistance. *Adv. Funct. Mater.* **2015**, *25*, 1527−1534.

(7) Kim, S.; Du, C.; Sheridan, P.; Ma, W.; Choi, S.; Lu, W. D. Experimental Demonstration of a Second-Order Memristor and Its Ability to Biorealistically Implement Synaptic Plasticity. *Nano Lett.* **2015**, *15*, 2203−2211.

(8) Abbas, Y.; Jeon, Y.-R.; Sokolov, A. S.; Kim, S.; Ku, B.; Choi, C. Compliance-Free, Digital SET and Analog RESET Synaptic Characteristics of Sub-Tantalum Oxide-Based Neuromorphic Device. *Sci. Rep.* **2018**, *8*, 1228.

(9) Kim, S. G.; Han, J. S.; Kim, H.; Kim, S. Y.; Jang, H. W. Recent Advances in Memristive Materials for Artificial Synapses. *Adv. Mater. Technol.* **2018**, *3*, 1800457.

(10) Mikawa, T.; Yasuhara, R.; Katayama, K.; Kouno, K.; Ono, T.; Mochida, R.; Hayata, Y.; Nakayama, M.; Suwa, H.; Gohou, Y.; Kakiage, T. Neuromorphic Computing Based on Analog ReRAM as Low Power Solution for Edge Application. In *2019 IEEE 11th International Memory Workshop (IMW); Monterey, USA, May 12−15*; IEEE, 2019; pp 1−4. DOI: 10.1109/IMW.2019.8739720.

(11) Zhang, W.; Gao, B.; Tang, J.; Li, X.; Wu, W.; Qian, H.; Wu, H. Analog-Type Resistive Switching Devices for Neuromorphic Computing. *Phys. Status Solidi RRL* **2019**, *13*, 1900204.

(12) Sangwan, V. K.; Hersam, M. C. Neuromorphic Nanoelectronic Materials. *Nat. Nanotechnol.* **2020**, *15*, 517−528.

(13) Liu, B.; Chang, K.; Yu, X.; Niu, Y.; Dong, X.; Wang, H. Compliance-Current Manipulation of Dual-Filament Switching in a $Ta/Ta_2O_5/In-Sn-O$ Structure with an Ultralow Power Consumption. *Phys. Rev. Appl.* **2021**, *16*, 044050.

(14) Ielmini, D. Resistive Switching Memories Based on Metal Oxides: Mechanisms, Reliability and Scaling. *Semicond. Sci. Technol.* **2016**, *31*, 063002.

(15) Lee, S. H.; Moon, J.; Jeong, Y.; Lee, J.; Li, X.; Wu, H.; Lu, W. D. Quantitative, Dynamic TaO_x Memristor/Resistive Random Access Memory Model. *ACS Appl. Electron. Mater.* **2020**, *2*, 701−709.

(16) Szot, K.; Dittmann, R.; Speier, W.; Waser, R. Nanoscale Resistive Switching in $SrTiO_3$ Thin Films. *Phys. Status Solidi RRL* **2007**, *1*, R86−R88.

(17) Lee, M.-J.; Han, S.; Jeon, S. H.; Park, B. H.; Kang, B. S.; Ahn, S.-E.; Kim, K. H.; Lee, C. B.; Kim, C. J.; Yoo, I.-K.; Seo, D. H.; Li, X.-S.; Park, J.-B.; Lee, J.-H.; Park, Y. Electrical Manipulation of Nanofilaments in Transition-Metal Oxides for Resistance-Based Memory. *Nano Lett.* **2009**, *9*, 1476−1481.

(18) Wedig, A.; Luebben, M.; Cho, D. Y.; Moors, M.; Skaja, K.; Rana, V.; Hasegawa, T.; Adepalli, K. K.; Yildiz, B.; Waser, R.; Valov, I. Nanoscale Cation Motion in TaO_x, HfO_x and TiO_x Memristive Systems. *Nat. Nanotechnol.* **2016**, *11*, 67−74.

(19) Moors, M.; Adepalli, K. K.; Lu, Q.; Wedig, A.; Bäumer, C.; Skaja, K.; Arndt, B.; Tuller, H. L.; Dittmann, R.; Waser, R.; Yildiz, B.; Valov, I. Resistive Switching Mechanisms on TaO_x and $SrRuO_3$ Thin-Film Surfaces Probed by Scanning Tunneling Microscopy. *ACS Nano* **2016**, *10*, 1481−1492.

(20) Yang, Y.; Zhang, X.; Qin, L.; Zeng, Q.; Qiu, X.; Huang, R. Probing Nanoscale Oxygen Ion Motion in Memristive Systems. *Nat. Commun.* **2017**, *8*, 15173.

(21) Yang, Y.; Huang, R. Probing Memristive Switching in Nanoionic Devices. *Nat. Electron.* **2018**, *1*, 274−287.

(22) Chen, S.; Jiang, L.; Buckwell, M.; Jing, X.; Ji, Y.; Grustan-Gutierrez, E.; Hui, F.; Shi, Y.; Rommel, M.; Paskaleva, A.; Benstetter, G.; Ng, W. H.; Mehonic, A.; Kenyon, A. J.; Lanza, M. On the Limits of Scalpel AFM for the 3D Electrical Characterization of Nanomaterials. *Adv. Funct. Mater.* **2018**, *28*, 1802266.

(23) Di Martino, G.; Demetriadou, A.; Li, W.; Kos, D.; Zhu, B.; Wang, X.; de Nijs, B.; Wang, H.; MacManus-Driscoll, J.; Baumberg, J. J. Real-Time in situ Optical Tracking of Oxygen Vacancy Migration in Memristors. *Nat. Electron.* **2020**, *3*, 687−693.

(24) Xiong, X.; Xiong, F.; Tian, H.; Wang, Z.; Wang, Y.; Tao, R.; Klausen, L. H.; Dong, M. Ultrathin Anion Conductors Based Memristor. *Adv. Electron. Mater.* **2022**, *8*, 2100845.

(25) Shi, Y.; Liang, X.; Yuan, B.; Chen, V.; Li, H.; Hui, F.; Yu, Z.; Yuan, F.; Pop, E.; Wong, H. S. P.; Lanza, M. Electronic Synapses Made of Layered Two-Dimensional Materials. *Nat. Electron.* **2018**, *1*, 458−465.

(26) Hui, F.; Liu, P.; Hodge, S. A.; Carey, T.; Wen, C.; Torrisi, F.; Galhena, D. T. L.; Tomarchio, F.; Lin, Y.; Moreno, E.; Roldan, J. B.; Koren, E.; Ferrari, A. C.; Lanza, M. In situ Observation of Low-Power Nano-Synaptic Response in Graphene Oxide Using Conductive Atomic Force Microscopy. *Small* **2021**, *17*, 2101100.

(27) Singh, R.; Kumar, M.; Iqbal, S.; Kang, H.; Kim, U.; Park, J.-Y.; Seo, H. Electric Field-Induced Area Scalability Toward the Multilevel Resistive Switching. *Adv. Mater. Interfaces* **2021**, *8*, 2100664.

(28) Lee, M.-J.; Lee, C. B.; Lee, D.; Lee, S. R.; Chang, M.; Hur, J. H.; Kim, Y.-B.; Kim, C.-J.; Seo, D. H.; Seo, S.; Chung, U. I.; Yoo, I.-K.; Kim, K. A Fast, High-Endurance and Scalable Non-Volatile Memory Device Made from Asymmetric Ta_2O_{5-x}/TaO_{2-x} Bilayer Structures. *Nat. Mater.* **2011**, *10*, 625−630.

(29) Jacobs, T. D. B.; Mathew Mate, C. M.; Turner, K. T.; Carpick, R. W. Understanding the Tip-Sample Contact. In *Scanning Probe Microscopy in Industrial Applications: Nanomechanical Characterization*; Yablon, D. G., Ed.; John Wiley & Sons, Inc.: Hoboken, 2013; pp 15−48. DOI: 10.1002/9781118723111.ch2
(30) Tseng, A. A.; Notargiacomo, A.; Chen, T. P. Nanofabrication by Scanning Probe Microscope Lithography: A Review. *J. Vac. Sci. Technol. B* **2005**, *23*, 877−894.
(31) Cambel, V.; Šoltýs, J. The Influence of Sample Conductivity on Local Anodic Oxidation by the Tip of Atomic Force Microscope. *J. Appl. Phys.* **2007**, *102*, 074315.
(32) Kim, T.; Son, H.; Kim, I.; Kim, J.; Lee, S.; Park, J. K.; Kwak, J. Y.; Park, J.; Jeong, Y. Reversible Switching Mode Change in Ta_2O_5-Based Resistive Switching Memory (ReRAM). *Sci. Rep.* **2020**, *10*, 11247.
(33) Miao, F.; Strachan, J. P.; Yang, J. J.; Zhang, M. X.; Goldfarb, I.; Torrezan, A. C.; Eschbach, P.; Kelley, R. D.; Medeiros-Ribeiro, G.; Williams, R. S. Anatomy of a Nanoscale Conduction Channel Reveals the Mechanism of a High-Performance Memristor. *Adv. Mater.* **2011**, *23*, 5633−5640.
(34) Li, S.; Liu, X.; Nandi, S. K.; Nath, S. K.; Elliman, R. G. Origin of Current-Controlled Negative Differential Resistance Modes and the Emergence of Composite Characteristics with High Complexity. *Adv. Funct. Mater.* **2019**, *29*, 1905060.
(35) Böttger, U.; von Witzleben, M.; Havel, V.; Fleck, K.; Rana, V.; Waser, R.; Menzel, S. Picosecond Multilevel Resistive Switching in Tantalum Oxide Thin Films. *Sci. Rep.* **2020**, *10*, 16391.
(36) Strukov, D. B.; Williams, R. S. Exponential Ionic Drift: Fast Switching and Low Volatility of Thin-Film Memristors. *Appl. Phys. A* **2009**, *94*, 515−519.
(37) Goldfarb, I.; Miao, F.; Yang, J. J.; Yi, W.; Strachan, J. P.; Zhang, M.-X.; Pickett, M. D.; Medeiros-Ribeiro, G.; Williams, R. S. Electronic Structure and Transport Measurements of Amorphous Transition-Metal Oxides: Observation of Fermi Glass Behavior. *Appl. Phys. A* **2012**, *107*, 1−11.
(38) Bondi, R. J.; Desjarlais, M. P.; Thompson, A. P.; Brennecka, G. L.; Marinella, M. J. Electrical Conductivity in Oxygen-Deficient Phases of Tantalum Pentoxide from First-Principles Calculations. *J. Appl. Phys.* **2013**, *114*, 203701.
(39) Xiao, B.; Watanabe, S. Oxygen Vacancy Effects on an Amorphous-TaO_x-Based Resistance Switch: A First Principles Study. *Nanoscale* **2014**, *6*, 10169−10178.
(40) Garg, S. P.; Krishnamurthy, N.; Awasthi, A.; Venkatraman, M. The O-Ta (Oxygen-Tantalum) System. *J. Phase Equilib.* **1996**, *17*, 63−77.
(41) Pedersen, C. S.; Chang, J. H.; Li, Y.; Pryds, N.; Garcia Lastra, J. M. Phase Separation in Amorphous Tantalum Oxide from First Principles. *APL Mater.* **2020**, *8*, 071108.
(42) Strukov, D. B.; Alibart, F.; Stanley Williams, R. S. Thermophoresis/Diffusion as a Plausible Mechanism for Unipolar Resistive Switching in Metal−Oxide−Metal Memristors. *App. Phys. A* **2012**, *107*, 509−518.
(43) Mickel, P. R.; Lohn, A. J.; Joon Choi, B. J.; Joshua Yang, J. J.; Zhang, M.-X.; Marinella, M. J.; James, C. D.; Stanley Williams, R. S. A Physical Model of Switching Dynamics in Tantalum Oxide Memristive Devices. *Appl. Phys. Lett.* **2013**, *102*, 223502.
(44) Ma, Y.; Li, D.; Herzing, A. A. A.; Cullen, D. A.; Sneed, B. T.; More, K. L.; Nuhfer, N. T.; Bain, J. A.; Skowronski, M. Formation of the Conducting Filament in TaO_x-Resistive Switching Devices by Thermal-Gradient-Induced Cation Accumulation. *ACS Appl. Mater. Interfaces* **2018**, *10*, 23187−23197.
(45) Xiao, B.; Yu, X.; Watanabe, S. A Comparative Study on the Diffusion Behaviors of Metal and Oxygen Ions in Metal-Oxide-Based Resistance Switches via ab Initio Molecular Dynamics Simulations. *ACS Appl. Electron. Mater.* **2019**, *1*, 585−594.
(46) Hur, J.-H. The Origin of the Exceptionally Low Activation Energy of Oxygen Vacancy in Tantalum Pentoxide Based Resistive Memory. *Sci. Rep.* **2019**, *9*, 17019.
(47) Kumar, S.; Graves, C. E.; Strachan, J. P.; Grafals, E. M.; Kilcoyne, A. L. D.; Tyliszczak, T.; Weker, J. N.; Nishi, Y.; Williams, R. S. Direct Observation of Localized Radial Oxygen Migration in Functioning Tantalum Oxide Memristors. *Adv. Mater.* **2016**, *28*, 2772−2776.
(48) Shannon, R. D. Revised Effective Ionic Radii and Systematic Studies of Interatomic Distances in Halides and Chalcogenides. *Acta Cryst. A* **1976**, *32*, 751−767.
(49) Heisig, T.; Lange, K.; Gutsche, A.; Goß, K. T.; Hambsch, S.; Locatelli, A.; Menteş, T. O.; Genuzio, F.; Menzel, S.; Dittmann, R. Chemical Structure of Conductive Filaments in Tantalum Oxide Memristive Devices and Its Implications for the Formation Mechanism. *Adv. Electron. Mater.* **2022**, *8*, 2100936.
(50) Yang, S. M.; Paranthaman, M. P.; Noh, T. W.; Kalinin, S. V.; Strelcov, E. Nanoparticle Shape Evolution and Proximity Effects during Tip-Induced Electrochemical Processes. *ACS Nano* **2016**, *10*, 663−671.
(51) Rezek, B.; Stuchlík, J.; Fejfar, A.; Kočka, J. Microcrystalline Silicon Thin Films Studied by Atomic Force Microscopy with Electrical Current Detection. *J. Appl. Phys.* **2002**, *92*, 587−593.
(52) Holm, R. Calculation of Constriction Resistances with Constant Resistivity ρ. In *Electric Contacts Handbook; Springer Berlin, Heidelberg*; Berlin/Heidelberg, 1958; pp 13−20. DOI: 10.1007/978-3-662-25893-4_4
(53) Fan, Y.-S.; Zhang, L.; Crotti, D.; Witters, T.; Jurczak, M.; Govoreanu, B. Direct Evidence of the Overshoot Suppression in Ta_2O_5-Based Resistive Switching Memory with an Integrated Access Resistor. *IEEE Electron Device Lett.* **2015**, *36*, 1027−1029.
(54) Spring, J.; Sediva, E.; Hood, Z. D.; Gonzalez-Rosillo, J. C.; O'Leary, W.; Kim, K. J.; Carrillo, A. J.; Rupp, J. L. M. Toward Controlling Filament Size and Location for Resistive Switches via Nanoparticle Exsolution at Oxide Interfaces. *Small* **2020**, *16*, 2003224.